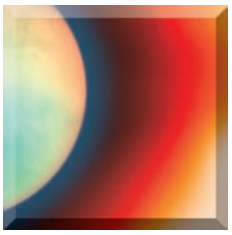

Space Weather Forecasting in the Exploration Era

David M. Rust, Manolis K. Georgoulis, Pietro N. Bernasconi, and Barry J. LaBonte

The nation's New Vision for Space Exploration program focuses on manned exploration, but before people can safely take extended trips outside Earth's protective magnetosphere, much better space weather forecasts of solar activity and its effects near Earth will be needed. The APL Solar Physics Section has developed several tools for interpreting solar observations that should lead to more accurate forecasts. These include automatic recognition of solar sigmoids, which frequently presage mass ejections from the Sun's atmosphere, and techniques for measuring the buildup of energy in electric currents over sunspots.

INTRODUCTION

The space between the Sun and the planets is filled with particles and fields that are constantly changing. Driven by solar events and modulated by planetary magnetic fields, this changing "space weather" affects humans and our technological systems. Solar events such as flares (Fig. 1) and coronal mass ejections (CMEs; Fig. 2) accelerate atomic particles to energies as high as 1 GeV, enough to penetrate any practical shielding that astronauts or spacecraft could carry. CMEs throw billions of tons of matter and entangled magnetic fields into interplanetary space at speeds up to 10 million km/h. When a CME hits Earth, it rattles the magnetosphere and induces ground currents that can overwhelm electric power distribution systems. Space storms also heat and inflate the atmosphere, thus altering spacecraft orbits; change the ionosphere, causing errors in GPS navigation; interrupt spacecraft operations by causing latch-ups in electronics; pose life-threatening radiation hazards to astronauts working outside the magnetosphere; and boost radiation in aircraft flying over the poles. Better engineering can mitigate many of these effects, but accurate forecasts of impending storms are still required to avoid costly downtime and life-threatening radiation hazards.

A goal of the APL Solar Physics Section is to improve our understanding of solar activity and how it affects the Sun–Earth system. We develop new instruments for measuring solar magnetism and radiation (see the article by Bernasconi et al., this issue) and analyze data from many solar observatories, both in space and on the ground, in addition to data from our own instruments. The focus is on understanding how solar magnetic fields can twist, merge, and destabilize to produce flares and CMEs, and we take both empirical and more rigorous scientific approaches to this research.

In this article, we describe examples of both approaches. First, we show empirical schemes to automatically recognize solar image patterns that are either precursors of an eruption or signatures that are helpful in forecasting the impact of the eruption on Earth.

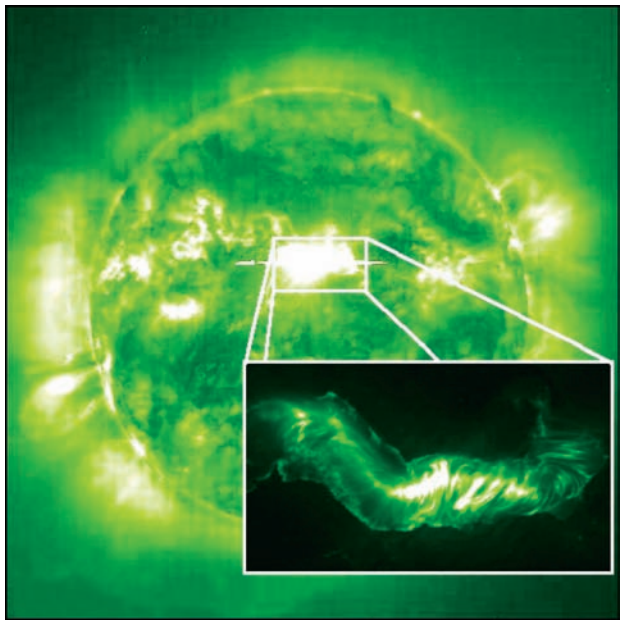

Figure 1. The giant "Bastille Day" flare at 10:36:10 UT on 14 July 2000. The inset shows details of the flare recorded by the TRACE (Transition Region and Coronal Explorer) spacecraft's Extreme-ultraviolet Imaging Telescope. The flare was so bright that details were lost in the full Sun image (background) recorded by the EUV telescope on the SoHO (Solar Heliospheric Observatory) spacecraft.

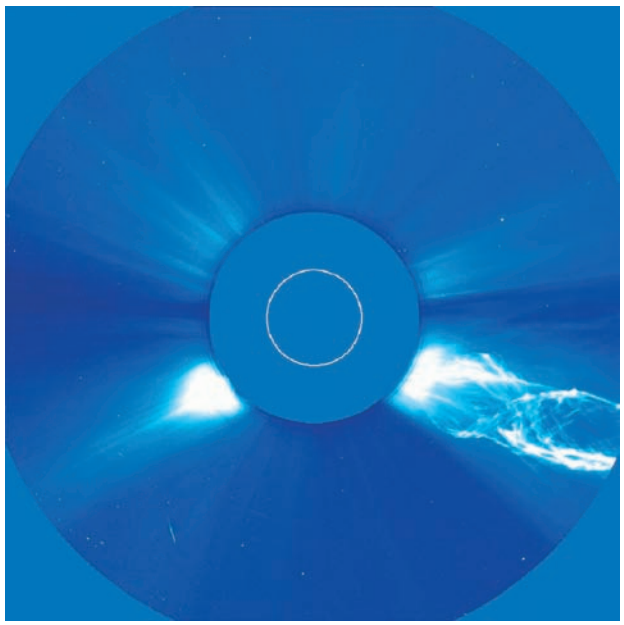

Figure 2. At 13:31:06 UT on 2 June 1998, the LASCO (Large Angle Spectroscopic Coronographs) white-light coronagraph on the SoHO spacecraft photographed a tangled CME (4 o'clock) from the Sun, which is occulted but represented by the white circle. The bright streamers are stable structures that rotate with the Sun.

Next, we show that many eruptions seem to involve the well-known magnetohydrodynamic kink instability,[1] which has its analog in common rubber bands: twist them enough and they kink. Finally, we discuss the physics-based methods we have developed to study magnetograms, which are maps of the direction and strength of the magnetic fields in so-called active regions (ARs) of the Sun, where flares and most CMEs originate. Many solar observatories make these maps every day, yet understanding how best to interpret them is still elusive.

AUTOMATED FEATURE RECOGNITION

Empirical models are really just probabilities that certain conditions will occur given the presence of a predictor—the "red sky at night, sailor's delight" approach. Empirical models of solar phenomena depend on measured properties of the Sun that presage violent events. While the human eye is a powerful filter to sort out interesting properties, it can be imprecise and variable in its performance. Our work emphasizes automated feature recognition algorithms to provide low operations cost and uniform performance. We illustrate here two examples of empirical forecast models.

Detecting Precursors of Coronal Mass Ejections

Progress in understanding CMEs has accelerated over the past decade because of the recognition that these eruptions spring from regions with twisted magnetic fields. A key signature of a twisted field is called a sigmoid. Figure 3 shows that a sigmoid is an S-shaped (sigmoidal) bright structure in the X-ray corona. Sigmoids become brighter and sometimes first appear just before CMEs and flares. Statistically, ARs with

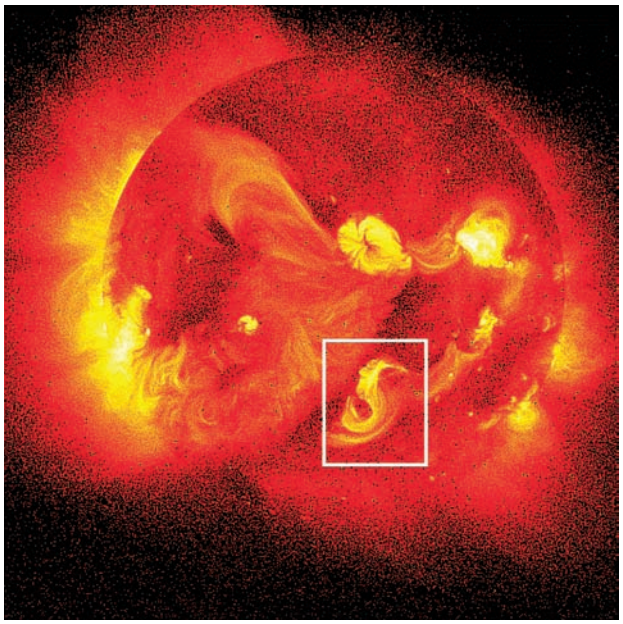

Figure 3. A bright sigmoid appeared in the southern solar hemisphere at 11:27 UT on 11 June 1992 in this image of the solar X-ray emissions taken with the Yohkoh/SXT.

sigmoidal coronal structure are more likely to have CMEs than those without.[2] Thus, the appearance of a sigmoid can be used in CME forecasts if an objective selection of features with sigmoidal shape can be devised. It makes physical sense that sigmoids would be associated with eruptions: in highly energized coronal states, with strong electric currents flowing, the overall shape of fields in an AR is theoretically sigmoidal.[3] The presence of a sigmoid is therefore an indicator that the coronal magnetic fields in ARs contain free magnetic energy that could be released in flares and CMEs.

Three studies of X-ray images like the one shown in Fig. 3 have produced the interesting result that most sigmoids have the same shape as kinked field lines. Theoretically, the critical sigmoid aspect ratio, length/width, is about 5.41. Measurements of more than 623 sigmoids have yielded an average aspect ratio of 5.47.[4,5] Allowing for projection effects, measurement uncertainties, and distortions of an ideal kink by real magnetic fields, we have to conclude that sigmoids signal the presence of kinked "flux ropes," in which the magnetic fields twist around each other as in a rope.

Given that sigmoids are important, how can we detect them automatically? Some detection problems are intrinsic to their nature. The correlation of structure and intensity is not straightforward, and sigmoids occur in many different sizes. Typical X-ray images have a dynamic range in intensity of hundreds to thousands. Even within a sigmoidal region, the intensity of the sigmoidal structure can vary widely. Therefore, any true sigmoid may be masked or a false sigmoid may be enhanced by errors in intensity scaling of the images. Another problem is that sigmoids visible at low resolution have variable structure at high resolution. Coupled with the range of potential sigmoid shapes, from an almost perfect "S" to less clear forms, reliable detection could depend on spatial resolution. Despite these many uncertainties, we developed consistent standards for sigmoid classification that are independent of image resolution and sigmoid intensity.

Within the context of the University Partnering for Operational Support (UPOS) program, we developed a software package that examines solar X-ray images and automatically detects AR sigmoids. The algorithm extracts key properties of the iso-intensity contours. In particular, the curvature of a sigmoidal contour as a function of arc-length has a unique form: large inward curvature at the ends and small outward curvature in the middle. Limits on the values of the curvature extrema and zero crossings unambiguously identify sigmoids over a wide range of forms. The process is independent of scale size because all dimensions are normalized to the contour length. To avoid foreshortening, the sigmoid detector algorithm restricts measurement to within 0.8 R_{sun} of disk center. The detector places limits on the size of contours to find sigmoids of AR size.

Figure 4 shows the results from the sigmoid detector for an image taken on 8 May 1992. The contours identifying sigmoids are plotted in black. The circle at 0.8 R_{sun} shows the limit of sigmoid detection. Beyond 0.8 R_{sun}, foreshortening makes it impossible to discern the true shape of the features. The sigmoid detector works well on Japan's Yohkoh/SXT (Soft X-ray Telescope) images, returning sigmoid identifications well away from the disk center, and since March 2003, it has been running in real time on images from the SXI (Solar X-ray Imager) telescope on a NOAA (National Oceanic and Atmospheric Administration) spacecraft. So far, hundreds of sigmoids have been detected and many warnings issued. Compilation of the eruptions actually associated with the warnings is in progress, but earlier studies showed that ARs with sigmoids are 68% more likely to be eruptive than nonsigmoidal regions.[2]

Solar Filament Classification

Filaments are thin threads of relatively dense, cool (10,000 K) gas suspended in the hot (1 million K) solar corona by a bundle of magnetic field lines twisted into a flux rope and arching up into the corona from the underlying photosphere. In images of the solar chromosphere (Fig. 5), which is a faint, thin, pink layer of the solar atmosphere above the familiar bright yellow photosphere, filaments can be clearly identified as dark, elongated features. They frequently stretch from tens of

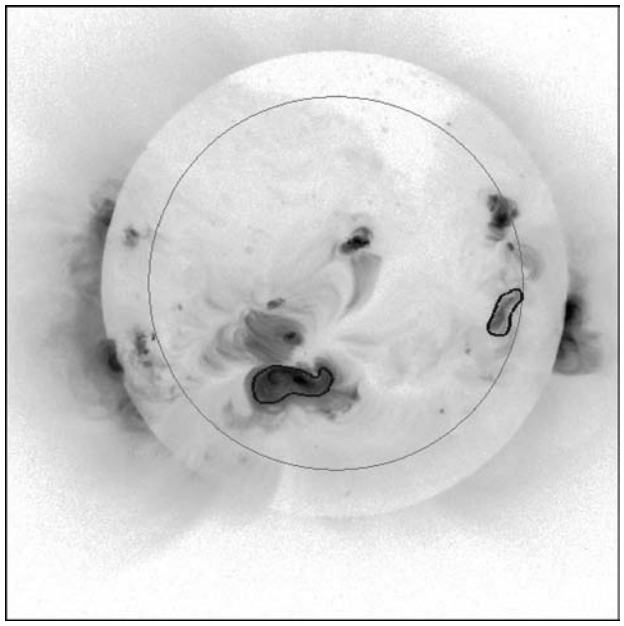

Figure 4. An example of the sigmoid detector response. Two sigmoids were found in this Yohkoh/SXT image at 11:05:46 on 8 May 1992: one near the central meridian and another near the west limb on the right. Black contours outline the sigmoids in this X-ray negative image. To avoid distortion by perspective effects, no attempt was made to detect sigmoids outside the light gray circle on this image, which shows faint structures better than a positive image does.

Figure 5. A dark filament observed in the southern solar hemisphere on 9 November 2002. Our automated filament recognition and characterization code autonomously detected the filament (outlined in yellow), determined its centerline (blue), and detected, classified, and counted its barbs (green lines). The code detected 1 unknown, 13 left-bearing, and no right-bearing barbs, which indicates that the filament was threaded by a right-handed magnetic flux rope.

thousands to several hundreds of thousands of kilometers. The magnetic flux ropes in which the filaments are embedded are just as long or longer.

A magnetic flux rope can have either a right- or left-handed twist. This twist defines the chirality (handedness) of the flux rope, which plays a role in determining the impact that it will have on Earth if it erupts and is ejected from the corona. During a CME, a magnetic flux rope and the dense material in the filament are both ejected from the Sun by magnetic forces and propelled into interplanetary space. CMEs that reach Earth can have a different impact on the magnetosphere, depending somewhat on the strength but mostly on the orientation of the magnetic fields carried by the CME. Knowing the geometry of the flux rope at the Sun before it erupts is thus important for predicting the geo-effectiveness of the CME. Unfortunately, it is very difficult to measure the magnetic field direction in a filament; however, from knowledge of the underlying fields, which is fairly easy to come by, and from the appearance of the filament, it is possible to derive the field direction and chirality.

Filaments show small appendages, called barbs, extending from their thin body (Fig. 5). A filament embedded in a right-handed helical flux rope exhibits mostly left-bearing barbs like left-lane exits on a freeway, while filaments within a left-handed flux rope show mostly right-bearing barbs. Therefore, by determining the direction of the barbs, one can infer the chirality of the magnetic flux rope. In the context of NASA's Living With a Star program, we developed a code for the automated detection and classification of filaments on the Sun. The program can autonomously and reliably detect filaments and determine their chirality by identifying right- and left-bearing barbs. For each filament on the solar disk, the code delivers some other relevant parameters, such as location, area, and average orientation, with respect to the equator. It can also track the day-by-day evolution of each filament as it rotates through the visible solar disk. Detecting filaments as they appear and tracking their evolution can help provide early warnings of potentially hazardous eruptions because nearly all filaments erupt at some point.

Recently we tested the filament classification code by analyzing daily images of the chromosphere taken at the Big Bear Solar Observatory in California from mid-2000 until mid-2004. The code identified more than 9000 filaments and established their chirality without human intervention. We compared the code results with a list of filament properties compiled manually at the National Solar Observatory in New Mexico over the same timeframe.[6] The computer list matched the observatory's list with a 72% success rate.

The results of our automated analysis program confirm previous findings, i.e., left-handed flux ropes predominate in the Sun's northern hemisphere and right-handed ones predominate in the south. We also found that filaments obeying this "hemispherical rule" tend to be larger and last longer before erupting than those that do not obey the rule. This result can be taken into account in integrated CME forecast programs that rely on many statistical relationships, such as the number of sunspots, presence of a sigmoid, chirality of the filaments, etc.

ANALYSIS OF SOLAR VECTOR MAGNETOGRAMS

Although the empirical approach to space weather forecasting may help with forecast accuracy in the short term, only an understanding of the basic physics of flares and CMEs will significantly improve forecast accuracy in the long term. Clearly, flares and CMEs are of magnetic origin. Assessing the magnetic fields in the solar atmosphere is, therefore, a central objective in understanding these phenomena. The magnetic fields are routinely measured only in the solar photosphere, and this severely limits our ability to understand and predict the evolution of the magnetic fields in the chromosphere and the corona. In addition, significant problems in the photospheric magnetic field measurements must be solved before any further analysis is performed.

Resolving Magnetic Field Direction Ambiguity

Photospheric vector magnetography uses the Zeeman effect[7] to measure the magnetic field along and transverse to the observer's line of sight. From these two components we can infer the magnetic field vector strength and direction at any strong-field location of the solar surface. While the magnitude of the transverse magnetic field is measured unambiguously, its azimuthal orientation is ambiguous, with two possible solutions differing by 180° owing to symmetries of the transverse Zeeman effect. Obviously, only one of the two solutions can be correct. This problem has been termed the *180° ambiguity* and is inherently nontrivial since single-height (photospheric) measurements preclude the application of the divergence-free (solenoidal) condition of the magnetic field vector to resolve the ambiguity. If vector magnetic fields are available for a succession of altitudes above the photosphere, then the ambiguity can, in principle, be solved exactly. We do not have this capability as yet, so the problem is ill posed, requiring physical assumptions and arguments to resolve the 180° ambiguity.

Most common attempts to resolve the 180° ambiguity rely on comparing the two possible solutions with simple magnetic field models and choosing the solution that matches the modeled fields most closely. This technique is acceptable for simple field configurations, but clearly fails in the complex, multipolar solar magnetic ARs that are most important in producing flares and CMEs. Another technique uses the concept of *simulated annealing*,[8] which simultaneously minimizes the current density and the divergence of the magnetic field vector, calculating all the possible combinations of these quantities. This technique is more physical, albeit computationally expensive, and requires hours of computing time per magnetogram. We introduced the *minimum structure* assumption: the sheath currents flowing between magnetic flux ropes in the solar atmosphere have a minimum magnitude.[9] That is, we assume that the magnetic fields in the solar atmosphere become as space filling (as unconstrained by currents) as possible, which is an intuitive choice for ARs on the Sun. This approximation allows the calculation of a vertical gradient of the magnetic field strength, thus providing some knowledge of the height variation of the magnetic field.

From this variation and the calculated vertical current density we obtain an initial solution of the 180° ambiguity for ARs. The final solution is reached by assuming smoothness of the azimuth solution. This minimizes the vertical current density and guarantees continuity of the resulting magnetic field vector. The minimum structure solution takes a few minutes of computing time per vector magnetogram and gives results that match our intuition about solar ARs.

Vertical Lorentz Forces and Cross-Field Electric Currents

Besides helping us to resolve the 180° ambiguity, the minimum structure approximation permits the calculation of the vertical Lorentz force $(\vec{J}\times\vec{B})_z$ (where $\vec{J}$ and $\vec{B}$ = the current density and the magnetic field vectors, respectively) on the plane of the magnetic field observations. Knowledge of the vertical Lorentz force then gives a lower limit for the cross-field electric current density, that is, the current density perpendicular to the magnetic field lines. These properties were never before measured on the photospheric plane, where it is believed that the Lorentz force is significant, so this exercise can be used to confirm or challenge the prevailing viewpoint.

We calculated the vertical Lorentz force and the minimum possible cross-field current from a number of AR vector magnetograms.[10] Both flaring and nonflaring ARs were used to uncover possible differences in terms of the "degree of force-freeness" in these ARs. In all cases we invariably found significant vertical Lorentz forces ranging from several hundredths to a few tenths of the photospheric gravitational force, and minimum cross-field current densities up to 35–45 mA m^{-2}. Flaring ARs tend to exhibit only slightly larger Lorentz forces and cross-field currents compared to nonflaring ARs. The typical vertical current density flowing along the field lines, on the other hand, was found to be 2–3 times smaller, on the order of 10–15 mA m^{-2}. The differences exceeded the associated uncertainties, so we safely conjecture that photospheric AR magnetic fields could not be force-free, in agreement with the prevailing viewpoint in solar physics.

Magnetic Helicity Flux and the Total Helicity Budget

Magnetic helicity is an important measure of the degree of twist and the number of interlinks in a magnetic field.[11] It tends to build up in the corona, that is, the fields there tend to become more twisted and intertwined with time because most of the magnetic fields emerging from below the photosphere are already twisted. Also, random shuffling motions in the photosphere tend to braid the overlying coronal fields because they all are rooted in the photosphere. Theoretically, we expect that the resulting helicity built up in the coronal magnetic fields can only be reduced by the ejection of the fields into interplanetary space. Indeed, estimates of the helicity injection rate are in good agreement with independent estimates of the helicity ejection rate,[12] so in hopes of finding a critical helicity flux rate that could be used to forecast eruptions, we instituted a program to measure the helicity flux.

Some measure of the helicity flux into the corona overlying ARs can be derived from the magnetograms obtained by the MDI (Michelson Doppler Imager)

aboard the SoHO spacecraft. We had to assume that most of the helicity comes from braiding and not from the emergence of twisted fields, that the magnetic field measurements are free of projection effects, and that the field motions in the photosphere can be tracked reliably.[13]

Although it is hard to test the validity of these assumptions, we proceeded anyway and studied 66 ARs with and without major flares. We found that the helicity injection rate averaged about twice as much in 34 ARs with one or more major flares and in 32 ARs without a major flare during the measurement interval. Since major flares are invariably accompanied by CMEs, this result tends to support the idea that CMEs are the mechanism by which the turbulent Sun eliminates the magnetic field twists and braids that inevitably build up in the corona.[14] But the result is of limited usefulness in flare forecasting, since the limiting assumptions and the method give only a helicity injection rate, not the net helicity accumulated. If we knew the helicity accumulated before each flare, it might provide some insight into a helicity threshold that could be used as a forecasting tool—something like the amount of stress required for an earthquake.

Calculating the total magnetic helicity accumulated in the corona above an AR is a completely intractable problem unless simplifying physical assumptions are used. The most common assumption is the force-free approximation: the electric current density is parallel with and proportional to the magnetic field, $\vec{J} = \alpha\vec{B}$. We use the linear force-free (α being constant) approximation, but we hope to upgrade to a nonlinear force-free (α being spatially variant) code eventually. Since we know that the photospheric AR magnetic fields are clearly forced, adopting any force-free approximation is an obvious compromise. However, the AR corona undergoes a dramatic change during an eruption, and we hope to replicate it, even with simplifying assumptions. Even if the value of our technique is limited when photospheric magnetograms are used, it is expected to be much greater in the future when chromospheric magnetograms become available, since the nonlinear force-free assumption is believed to be valid in the chromosphere.

Our technique starts with the energy equation in an isolated magnetic structure, where the total magnetic energy is the sum of the magnetic energy of the current-free (i.e., vacuum) magnetic field and the free magnetic energy induced by electric currents ($E_{\text{total}} = E_{\text{vacuum}} + E_{\text{free}}$). The energy of the vacuum field is not available for release, but the free energy may be. In the linear force-free approximation, the energy formula becomes the energy-helicity formula,[15] with the free magnetic energy in 1:1 correspondence with the magnetic helicity H:

$$E_{\text{total}} = E_{\text{vacuum}} + \frac{\alpha}{8\pi} H. \tag{1}$$

Although it is possible to obtain a volume integral for the total helicity H, its evaluation in modeled coronal magnetic fields of solar ARs is susceptible to systematic effects in the extrapolation methods. Therefore, a goal would be to express each term in Eq. 1 as an integral on the solar surface. It is easy to do that for the vacuum field energy, while the total helicity can be expressed in similar terms by realizing that the linear force-free magnetic energy is the minimum energy of a magnetic structure with a given amount of magnetic helicity in the structure.[16] This helicity is prescribed by the constant force-free parameter α. In conclusion, we find

$$E_{\text{total}} = (1 + b_0 N^2) E_{\text{vacuum}}, \tag{2}$$

$$H = 8\pi L b_0 N E_{\text{vacuum}}, \tag{3}$$

and

$$E_{\text{vacuum}} = \frac{1}{8\pi} \int_S \vec{B}_{\text{p}} \times \vec{A}_{\text{p}} \cdot \hat{\xi}\, dS, \tag{4}$$

where

b_0 = a constant related to the ratio of the vacuum field energy to the linear force-free field energy,

N = the number of turns in the AR,

L = the length of the AR,

$\vec{B}_{\text{p}}$ = the vacuum magnetic field,

$\vec{A}_{\text{p}}$ = the magnetic field vector potential, i.e., $\vec{\nabla} \times \vec{A}_{\text{p}} = \vec{B}_{\text{p}}$, and

the integration surface S corresponds to the boundary (photospheric) plane for which magnetic field measurements exist.

Equations 2–4 rely on the linear force-free approximation, but they can be used in a nonlinear force-free approach by assuming that the linear force-free approximation holds for each individual magnetic field line rooted in the photosphere and then by integrating all the elementary current-free field energies, total energies, and field-line helicities on the photospheric plane. The force-free parameter α for each field line can be calculated by observations.

Examples of Vector Magnetogram Analysis

What do these physical models teach us about forecasting space weather? The following two examples of flare-productive ARs illustrate the quantitative analysis that is now possible.

The first example is NOAA AR 8210 on 1 May 1998. This AR showed a very complex magnetic configuration with a rotating sunspot and gave a number of flares and CMEs during its passage from the solar disk (background of Fig. 6). We analyzed the vector magnetograms

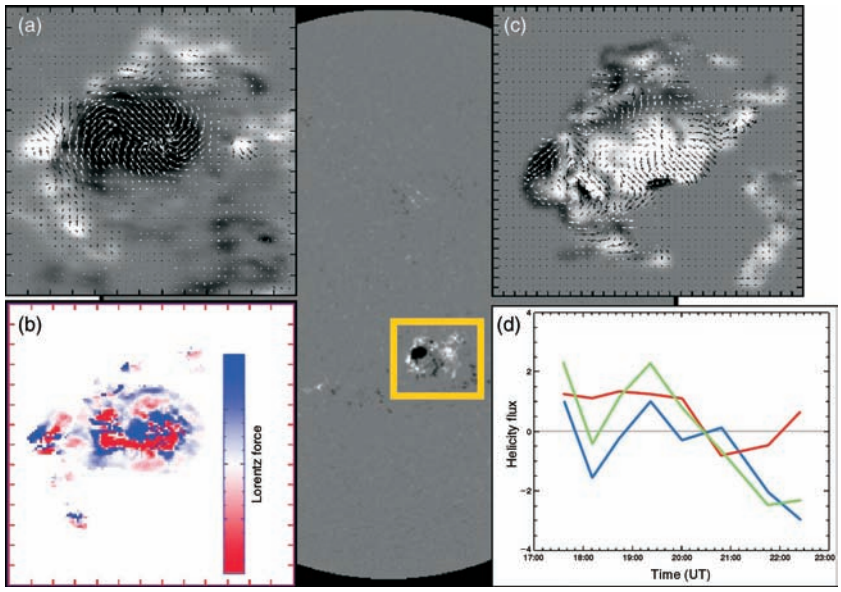

Figure 6. Vector magnetogram analysis in NOAA AR 8210 on 1 May 1998. The location of the AR on the solar disk is shown in the full-disk magnetogram of the SoHO/MDI (background). (a) The minimum structure ambiguity-free magnetic field vector in the AR. (b) The Lorentz force calculated in the main sunspot of the AR. (c) The average inductive velocity field vector calculated for the AR. (d) The helicity flux in the AR. Shown are the injected helicity flux (red), the helicity flux generated by photospheric shuffling (blue), and the total helicity flux (green). Tick mark separation is 7000 km in Figs. 6a and 6b and 3500 km in 6c.

produced by the IVM (Imaging Vector Magnetograph) of the University of Hawaii. The minimum structure ambiguity-free magnetic field vector in the AR photosphere is given in Fig. 6a. Figure 6b shows an image of the Lorentz force in the AR. The sunspot area exhibits strong Lorentz forces. Figure 6c shows an average of our minimum structure velocity field reconstruction. This is another of our techniques for solving the ideal induction equation for a pair of vector magnetograms, thereby calculating the flow field required to explain the evolution seen from the first magnetogram to the second. Several details of the flows in the AR are reproduced, including sunspot inflows/outflows and velocity shear along a polarity reversal line at the left of the sunspot. In Fig. 6d we show the two terms of the helicity flux in the AR photosphere, namely, helicity injection (red line) and helicity generation by photospheric shuffling (blue line). The green line corresponds to the total helicity flux in the AR. We notice that the injected helicity flux is more consistent than the generated helicity flux and changes sign from positive (right-handed helicity) to negative (left-handed helicity) during the observing interval. This behavior prompts the total helicity flux to change sign as well. Simultaneously present opposite senses of helicity is a feature acknowledged by several theorists as a sign of an imminent eruption. Indeed, approximately 30 min after this behavior stopped for the injected helicity flux, a CME-triggering solar flare occurred in the AR. We have found that the subregion of the AR in which the injected helicity flux changed sign coincided with the origin location of the flare.

The next example is NOAA AR 10030 on 15 July 2002. The AR gave at least two X-ray flares and triggered a CME during the observing interval. The time series of the total magnetic energy is shown in Fig. 7a, while the time series of the total magnetic helicity in the AR is given in Fig. 7b. The two parallel blue lines indicate the onset time of the two major flares. Figure 7c shows a snapshot of the CME that was related to the X3 flare and appeared in the field of view of the SoHO/LASCO coronagraph approximately 1 h after the flare.

Figures 7a and 7b clearly show that the total magnetic energy, as well as the absolute value of the total magnetic helicity in the AR, was decreasing during the IVM observations. Since the current-free magnetic energy cannot be released, the decrease in total energy implies that the free magnetic energy of the AR is released. This is in concert with the triggering of the two flares. The decrease of helicity has further consequences: Since magnetic helicity is a globally conserved quantity, a decrease in absolute values means that a part of the magnetic configuration lost its connection with the photospheric boundary, either by descending back into the solar interior or by ejecting into the heliosphere. The onset of the CME clearly indicates that part of the AR corona was blown away. The observed change in helicity in Fig. 7b may then be used as a proxy of the helicity content of the CME. We found that this CME was a left-handed helical magnetic structure with a total helicity content of -4×10^{43} Mx^2. Based on the location of the AR on the solar disk when the CME was triggered, one may infer that the front side of the propagating magnetic structure should show a southward component of its magnetic field vector when it reaches the terrestrial magnetosphere. A southward component can induce a geomagnetic storm, and this occurred about 4–5 days after the CME. In Fig. 7c we show the measured and predicted geomagnetic Dst index. The blue line indicates the onset of the CME late on 15 July 2002, while a moderate geomagnetic storm (-40 nT < Dst < -20 nT) set in between 20 and 23 July 2002 (indicated by the blue oval).

These examples showcase the potential of our vector magnetogram analysis techniques for understanding solar flares and CMEs. Even the compromising linear force-free approximation might provide insight into the physical processes at work. The value of our technique

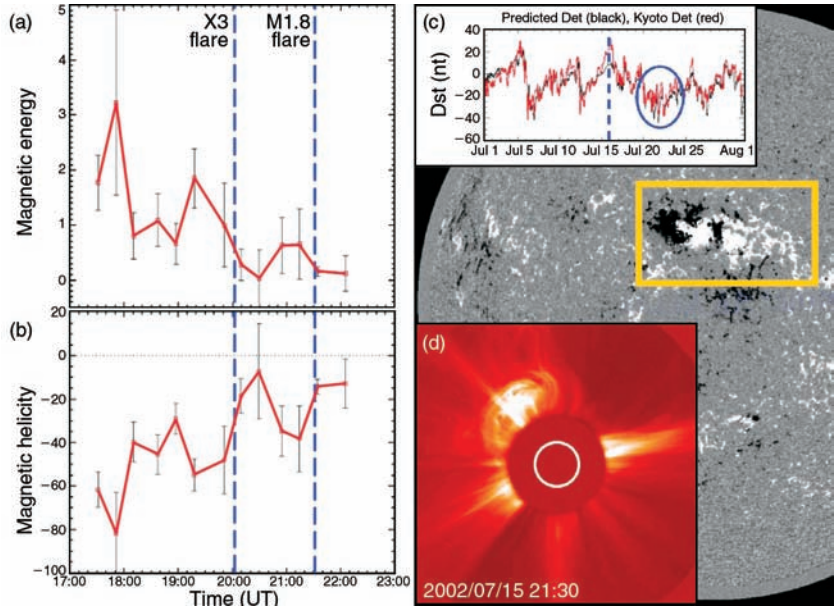

Figure 7. Vector magnetogram analysis in NOAA AR 10030 on 5 July 2002. The location of the AR on the solar disk is shown in the full-disk magnetogram of the SoHO/MDI (background). (a) Time series of the total magnetic energy. (b) Time series of the total magnetic helicity. The two parallel blue lines in Figs. 7a and 7b indicate the onset times of two major X-ray flares. (c) The triggering of a geomagnetic disturbance caused by the CME shown in Fig. 7d. (d) SoHO/LASCO coronagraph image of the CME related to the X3 flare.

will increase significantly when the nonlinear force-free approximation is used.

The application of our analyses to nonflaring ARs without CMEs also yielded interesting results: We found that in flare-/CME-prolific ARs, the percentage of the free magnetic energy is typically ≈15% or larger of the total magnetic energy in the AR, whereas in nonflaring ARs the percentage is typically 5% or lower. For NOAA ARs 8210 and 10030, the percentages were 14 and 27%, respectively. This relatively large percentage of free energy illustrates the complexity of the flaring ARs and favors the triggering of eruptions. In terms of the total magnetic helicity, eruptive ARs have a 5–10 times larger helicity budget than nonflaring ARs. We are currently seeking more examples of vector magnetograms of flaring and nonflaring ARs to improve the statistical significance of our conclusions.

CONCLUSION

To provide more reliable 3- to 7-day forecasts of large geomagnetic storms, we have developed a number of stand-alone products: the sigmoid detector and filament classifier codes and a toolbox of codes for analyzing solar magnetograms. Currently only one of these products is operating in real time: the sigmoid detector is coupled with an estimate of the probability of a CME, based on the published statistical association.[2] This system operates on images from the NOAA GOES spacecraft or from the NASA/European Space Agency SoHO spacecraft (see http://sd-www.jhuapl.edu/UPOS/CME/index.html).

Since magnetic helicity is ejected from the Sun with each CME, any estimate of magnetic helicity transfer provides a potentially useful early indicator that a CME may occur. Initial tests of the helicity transfer program based on analyses of SoHO magnetograms have been completed, and a product that automatically evaluates relative helicity buildup will be operational on the UPOS website in 2006. This approach to helicity buildup has the advantage of requiring only SoHO or equivalent magnetograms. It has the disadvantage that it estimates only one component of helicity transfer. So we will integrate our existing prediction products with more sophisticated tools for analyzing full vector magnetograms. Previous techniques for resolving the 180° ambiguity require hours of computing time per vector magnetogram, but our solution is reached in 10 min for the same targets. Since it is fast and fully automatic, our "structure minimization" technique can expedite the resolution of solar vector magnetograms into a near-real-time process.

Once the azimuthal ambiguity has been removed, a time series of vector magnetograms can be used to calculate the total helicity transfer rate to help forecast CMEs. The existing code needs to be modified to calculate the magnetic field configuration above each AR so that a forecast of the magnetic structure of any CMEs aimed at Earth can be integrated into the final product. This is important since southward-directed fields produce major geomagnetic storms. Fully integrated forecasts will include an estimate of the likelihood of an extended period of strong southward-directed fields striking Earth's magnetosphere.

Our product will take advantage of several important new data sources when they come online. We can use the SoHO data for sigmoids, but early next year the STEREO (Solar TErrestrial RElations Observatory) mission will be launched. STEREO will provide sigmoid data from two important new vantage points: one is above the east limb of the Sun where sigmoids that will influence space weather in the coming week can be seen more clearly than from Earth, and the other is above the west limb of the Sun where the origins of the most hazardous solar energetic particle events can best be seen. We can implement our forecast product

as soon as STEREO is launched and provide real-time forecasts for years. This will be a first test of the future systems needed for forecasting space weather throughout the solar system, wherever spacecraft and astronauts venture to explore.

ACKNOWLEDGMENTS: This article is dedicated to our gifted colleague, Barry J. LaBonte, who passed away on 24 October 2005 and who led our efforts to develop automated solar event detection for space weather forcasting. His expertise and good fellowship will be sorely missed. We are grateful to the SoHO consortium for use of their data and wonderful solar images. SoHO is a project of international cooperation between ESA and NASA. We also thank the ISAS/NASA Yohkoh SXT telescope team and the University of Hawaii Mees Solar Observatory for their data. Various programs, notably NASA's Living With a Star and the Solar and Heliospheric Physics programs, supported the work reported here. We are grateful also to the UPOS program.

REFERENCES

[1]Baty, H., Einaudi, G., Lionello, R., and Velli, M., "Ideal Kink Instabilities in Line-Tied Coronal Loops," *Astron. Astrophys.* **333**, 313–321 (1998).
[2]Canfield, R. C., Hudson, H. S., and McKenzie, D. E., "Sigmoidal Morphology and Eruptive Solar Activity," *Geophys. Res. Lett.* **26**, 627 (1999).
[3]Amari, T., Luciani, J. F., Mikic, Z., and Linker, J., "A Twisted Flux Rope Model for Coronal Mass Ejections and Two-Ribbon Flares," *Astrophys. J.* **529**, L49–L52 (2000).
[4]Rust, D. M., and Kumar, A., "Evidence for Helically Kinked Magnetic Flux Ropes in Solar Eruptions," *Astrophys. J.* **464**, L199–L202 (1996).
[5]Leamon, R. J., Canfield, R. C., Blehm, Z., and Pevtsov, A. A., "What Is the Role of the Kink Instability in Solar Coronal Eruptions?" *Astrophys. J.* **596**, L255–L258 (2003).
[6]Pevtsov, A. A., Balasubramaniam, K. S., and Rogers, J. W., "Chirality of Chromospheric Filaments," *Astrophys. J.* **595**, 500–505 (2003).
[7]Stenflo, J. O., "Hanle-Zeeman Scattering Matrix," *Astron. Astrophys.* **338**, 301–310 (1998).
[8]Metcalf, T. R., "Resolving the 180-Degree Ambiguity in Vector Magnetic Field Measurements: The 'Minimum' Energy Solution," *Solar Phys.* **155**, 235–242 (1994).
[9]Georgoulis, M. K., LaBonte, B. J., and Metcalf, T. R., "On the Resolution of the Azimuthal Ambiguity in Vector Magnetograms of Solar Active Regions," *Astrophys. J.* **602**, 446 (2004).
[10]Georgoulis, M. K., and LaBonte, B. J., "Vertical Lorentz Force and Non-Field-Aligned Currents in the Photospheric Magnetic Fields of Solar Active Regions," *Astrophys. J.* **615**, 1029 (2004).
[11]Berger, M. A., and Field, G. B., "The Topological Properties of Magnetic Helicity," *J. Fluid Mech.* **147**, 133–148 (1984).
[12]Bieber, J. W., and Rust, D. M., "The Escape of Magnetic Flux from the Sun," *Astrophys. J.* **453**, 911 (1995).
[13]Chae, J., "Observational Determination of the Rate of Magnetic Helicity Transport Through the Solar Surface via the Horizontal Motion of Field Line Footpoints," *Astrophys. J.* **560**, L95–L98 (2001).
[14]Rust, D. M., "Spawning and Shedding Helical Magnetic Fields in the Solar Atmosphere," *Geophys. Res. Lett.* **21**, 241–244 (1994).
[15]Berger, M. A., "An Energy Formula for Nonlinear Force-Free Magnetic Fields," *Astron. Astrophys.* **201**, 355–361 (1988).
[16]Woltjer, J., "A Theorem on Force-Free Magnetic Fields," *Proc. Nat. Acad. Sci. USA* **44**, 489 (1958).

THE AUTHORS

David M. Rust leads the Space Department's Solar Physics Section. Dr. Rust is a Principal Professional Staff member who initiated the research programs on solar sigmoids and filaments and magnetic fields. He served as chair of the NASA team that defined the STEREO mission, a major spacecraft project now being implemented at APL for understanding the origins and effects of solar activity. Through an analysis of solar images, he discovered evidence for magnetohydrodynamic kink instabilities in the solar atmosphere. **Manolis K. Georgoulis** is a member of the Senior Professional Staff in the Space Department and the Principal Investigator on a study of mechanisms to heat the solar atmosphere. Dr. Georgoulis is also a Co-Investigator on a project to determine the magnetic helicity flux through solar active regions, and has developed several new methods for resolving ambiguities in solar magnetic field measurements. **Pietro N. Bernasconi** leads our effort to automate the analysis of solar images. Dr. Bernasconi is a member of the Senior Professional Staff in the Space Department. He has extensive experience in the analysis of solar vector magnetic field measurements obtained from ground-based and balloon-borne telescopes. **Barry J. LaBonte**, who died tragically on 24 October 2005 of complications following surgery, led the Solar Physics Section's efforts to calculate the helicity flux in solar active regions. Dr. LaBonte was a member of the Principal Professional Staff. Before coming to APL, he was Professor of Astronomy at the University of Hawaii. Further information on the work of the Solar Physics Section can be obtained from David Rust. His e-mail address is david.rust@jhuapl.edu.


David M. Rust


Manolis K. Georgoulis


Pietro N. Bernasconi


Barry J. LaBonte